

# Towards an Efficient Optimization-based Framework for Selecting Under-frequency Load Shedding Parameters

Mazen Elsaadany  
University of Vermont  
[melsaada@uvm.edu](mailto:melsaada@uvm.edu)

Waheed Owonikoko  
University of Vermont  
[waheed.ownonikoko@uvm.edu](mailto:waheed.ownonikoko@uvm.edu)

Amritanshu Pandey  
University of Vermont  
[amritanshu.pandey@uvm.edu](mailto:amritanshu.pandey@uvm.edu)

Mads R. Almassalkhi  
University of Vermont  
[malmassa@uvm.edu](mailto:malmassa@uvm.edu)

## Abstract

*High penetration of renewable resources is resulting in a power system with a lower inertia and higher frequency sensitivity to power imbalances. Such systems are becoming increasingly susceptible to frequency collapse during extreme disturbances. Under Frequency Load Shedding (UFLS) is a last resort protection scheme for such scenarios, and it acts as an emergency brake by shedding load to arrest frequency decline. Current and emerging efforts to optimize UFLS settings and frequency thresholds are mostly network agnostic, ignoring spatial information about the network. With the prevalence of Distributed Energy Resources (DERs) in the high-renewable paradigm, the power grid is becoming more bidirectional, making some locations in the network more effective for UFLS action than others. This work proposes a Mixed Integer Linear Program that optimizes the UFLS setpoints (prioritizing one location over another) to minimize frequency deviation and load-shed for a given disturbance. The formulation considers system information and DER generation mix at different network locations, increasing model fidelity. The formulation also captures the discrete nature and practical time delays and deadbands associated with UFLS using half as many binary variables, reducing problem complexity. We empirically validate the optimization approach on a WECC 9 bus system and a 45-bus system for performance metrics including frequency deviation, frequency nadir, steady-state frequency and solver time.*

**Keywords:** Under-frequency Load Shedding, Mixed Integer Optimization, Power System Stability, Distributed Energy Resources

## 1. Introduction

The amount of renewable energy resources (RES) being integrated into the power grid has been on the rise in recent years. This has caused the system inertia to decrease, resulting in larger frequency sensitivity to power imbalances. This

makes the system more prone to underfrequency events due to disturbances like the loss of a major generator that can cause a rapid fall in frequency, leading to a blackout if not dealt with promptly. To avoid the frequency decreasing to an undesirable level possibly leading to system instability or blackout, appropriate control measures must be established. Under-frequency load shedding (UFLS) is the electricity system's emergency control mechanism Kundur, 1994 designed to arrest frequency decline during large/extreme under-frequency events by shedding load and easing imbalance between generation and demand.

UFLS can be divided into two main categories, i) conventional UFLS, which entails shedding a certain (pre-defined) amount of load at specified frequency thresholds, ii) adaptive UFLS schemes which shed load based on the rate of change of frequency (RoCoF) and/or the frequency deviation Ghaderi Darebaghi and Amraee, 2017; Liu et al., 2014; Rudez and Mihalic, 2016; Sun et al., 2021. Note, that adaptive UFLS schemes can later be classified into several sub-categories. The main theme in all adaptive UFLS schemes is that the RoCoF and the frequency are used to infer the magnitude of the disturbance causing the frequency decline which is then used to determine the load shed.

Each UFLS type has its shortcomings; for the conventional UFLS scheme, the condition used as the baseline for the scheme design may be significantly different than the condition under which it may operate. This may lead to over or under-shedding of load Adiyabazar et al., 2020; He et al., 2019; Rudez and Mihalic, 2016; Sigrist et al., 2012. Many current adaptive UFLS schemes are also prone to shedding sub-optimally since locally measured frequency and RoCoF obtained cannot fully describe all the system frequencies, and the center of inertia (CoI) RoCoF is needed to infer the disturbance magnitude better to approximate the appropriate amount of load-she Milano, 2017. Furthermore, to accurately measure the CoI RoCoF phasor measurement units (PMU) are needed at all generator buses in the system (adding to the cost). Also, high communication overhead is accrued since

all frequency measurements are needed to calculate the CoI RoCoF.

Many conventional UFLS scheme-based methods have been proposed in recent literature. Tofis et al., 2016 employs swing equation dynamics to minimize the load shed amount while ensuring system frequency remains within acceptable transient and steady-state limits. Note, in this approach, the load is shed all at once after the disturbance. The authors in Ceja-Gomez et al., 2012; Rafinia et al., 2020 and Amraee et al., 2017 present a Mixed Integer Linear Program (MILP) formulation to optimally obtain frequency thresholds and load shedding amount for each stage. The work optimizes the setpoints in a conventional UFLS setting, considering time delay, system inertia, damping, and uncertainty from solar PV generation.

Several adaptive UFLS schemes have also been proposed. In Sun et al., 2021, the author suggests a method for approximating the CoI RoCoF from local measurements based on the inflection points of the local frequency. In Zuo et al., 2019, a RoCoF-based local UFLS system was proposed; this method estimates RoCoF and frequency using PMU measurements which are then used to determine the amount of load to be shed. In Terzija, 2006, the author presents a nonrecursive Newton-type approach for estimating frequency and RoCoF. The frequency and RoCoF estimates are further used to estimate the size and location of the disturbance. In this approach, the amount of load shed is based on the disturbance size and location estimates. RoCoF estimates can be subject to error since second derivatives of frequency measurements are involved, making estimates prone to noise, potentially leading to over/under load shedding.

One prevalent drawback of the UFLS schemes proposed in the literature is that they are network agnostic and do not consider network spatial information. With increased penetration of DER generation in the grid, the power system is becoming more bidirectional, with some areas having DER generation that exceeds demand. This results in backfeeding, and triggering a UFLS relay at such locations would lead to a counter productive loss of generation. Therefore, network spatial information as well as information about DER generation should be considered in emerging UFLS scheme design by including a higher-fidelity grid model.

While MILP-based formulations have been used for UFLS scheme design Amraee et al., 2017; Rafinia et al., 2020, they have been network agnostic and questions of where to shed the load, how much load should be shed, and whether some buses are more suitable for UFLS than others are still unanswered. Hence, this work proposes an optimization framework wherein UFLS setpoints are adapted regularly by considering changing grid conditions, network spatial information and DER generation information to UFLS scheme-design. The paper's contributions are summarized as follows:

- 1. Improved model fidelity:** We design a high-fidelity UFLS scheme with a MILP-based optimization that incorporates the network spatial information to optimize UFLS parameters. The formulation incorporates information

about DER generation at various bus locations to mitigate the adverse effects of triggering a UFLS relay at locations where backfeeding occurs.

- 2. Reducing solution complexity:** We reduce complexity in MILP formulation by using a single binary variable to a) indicate when the frequency is below the threshold and b) when the load-shedding action is activated.
- 3. Empirical validation:** We demonstrate the efficacy and benefits of our proposed approach with simulation-based analysis of 9-bus and 45-bus dynamic test cases.

The rest of the paper is arranged as follows: Section 2 describes the dynamic model used in the UFLS scheme design. Section 3 validates the dynamics model. Section 4 describes the problem formulation. Section 5 covers the methodology. Section 6 and Section 7 discuss the results and conclusion, respectively.

## 2. System Modeling

The bulk power system dynamics are governed by AC power flow equations, swing equations, generator governor and turbine dynamics, automatic voltage regulators, and load models. For the analysis in this paper, we adopt a simplified dynamics model of the power grid that considers the generator governor, swing equations, and DC power flow equations. In Section 3, we evaluate the efficacy of this simplified model against the nonlinear model. The simplified system model is adapted from Poola et al., 2018 and Figliolo and Giusto, 2020. In the model, the deviations in voltage phase angle and angular frequency from nominal, at each bus  $i \in \mathcal{B} := \{1, \dots, N\}$ , are denoted by  $\theta^i$  and  $\omega^i$ , respectively. That is, at nominal steady state conditions,  $\theta^i = 0$  and  $\omega^i = 0$ .

Let a power system be described by a weighted graph  $\mathcal{G} = (\mathcal{B}, \mathcal{E})$ .  $\mathcal{B}$  is the set of buses composed of the union of disjoint sets of generator ( $\mathcal{B}_G$ ) and non-generator ( $\mathcal{B}_L$ ) buses, i.e.  $\mathcal{B} = \mathcal{B}_G \cup \mathcal{B}_L$  and  $\mathcal{B}_G \cap \mathcal{B}_L = \emptyset$ .  $\mathcal{E}$  denotes the transmission lines connecting the buses in the network, each line is weighted with its corresponding line susceptance. Let the number of buses in the system be  $N$  and the number of edges (transmission lines) be  $N_e$ . The node arc incidence matrix ( $C$ ) is a  $N \times N_e$  matrix defined as follows:

$$C_{je} = \begin{cases} 1 & \text{if node } j \text{ is the source of edge } e \\ -1 & \text{if node } j \text{ is the sink of edge } e \\ 0 & \text{otherwise} \end{cases} \quad (1)$$

Let the matrix  $B_e$  be an  $N_e \times N_e$  diagonal matrix with the diagonal entries being the line susceptances  $B_{ij}$ . The weighted graph Laplacian matrix,  $L \in S^n$  where  $S^n$  is the set of symmetric  $n \times n$  matrices, can be defined as follows:

$$L = CB_e C^T \quad (2)$$

Thus, let  $\theta_G$  and  $\omega_G$  denote vectors containing the angles and frequencies of generator buses while  $\theta_L$  and  $\omega_L$  denote vectors of angles and frequencies at non-generator buses.

Collating these vectors yields the full network's bus angles and frequencies

$$\theta = \begin{bmatrix} \theta_G \\ \theta_L \end{bmatrix}, \quad \omega = \begin{bmatrix} \omega_G \\ \omega_L \end{bmatrix}. \quad (3)$$

To incorporate the dynamics of generator bus angles and frequencies, the swing equations are used:

$$\dot{\theta}_G^i = 2\pi f_{\text{base}} \omega_G^i \quad \forall i \in \mathcal{B}_G \quad (4)$$

$$M^i \dot{\omega}_G^i = P_{\text{Line}}^i - D^i \omega_G^i + P_m^i + P_{\text{sh}}^i + \eta^i, \quad \forall i \in \mathcal{B}_G \quad (5)$$

where  $M$  and  $D$  are the generator inertia and damping coefficient, respectively,  $P_{\text{Line}}^i$  is the deviation in the net power injection to bus  $i$  from nominal, and  $P_m^i$  is the deviation in generator mechanical power input from nominal and driven by the governor. The load shed at bus  $i$  is denoted  $P_{\text{sh}}^i$ . If a bus does not have load or is not participating in the UFLS scheme, then the corresponding  $P_{\text{sh}}^i$  is omitted. As part of the manuscript's focus on UFLS, we consider the system's response to large disturbances at bus  $i$ , which is denoted  $\eta^i$ . The base frequency is denoted  $f_{\text{base}}$  and is in Hz. Note, a factor of  $2\pi f_{\text{base}}$  is needed in (4) since the frequency is in per unit and the bus angle is in radians. The mechanical power input to the generator  $i$  from the governor is modeled as a first order low pass filter, as shown below:

$$P_m^i(s) = -\frac{K_{\text{gov}}^i}{T_{\text{gov}}^i s + 1} \omega^i, \quad (6)$$

where  $K_{\text{gov}}^i$  is the governor gain, and  $T_{\text{gov}}^i$  is the governor time constant. In time domain, the mechanical power input,  $P_m^i(t) = -K_{\text{gov}}^i x_{\text{gov}}^i(t)$ , yields governor dynamics:

$$\Rightarrow \dot{x}_{\text{gov}}^i = \frac{1}{T_{\text{gov}}^i} \omega_G^i - \frac{1}{T_{\text{gov}}^i} x_{\text{gov}}^i \quad \forall i \in \mathcal{B}_G. \quad (7)$$

The change in net power flowing into bus  $i$  is a function of the change in sum of line flows:

$$P_{\text{Line}}^i = - \sum_{j \in \mathcal{N}_i} P_{ij}, \quad \forall i \in \mathcal{B} \quad (8)$$

where  $P_{ij}$  is the line flow from bus  $i$  to bus  $j$  and  $\mathcal{N}_i \subset \mathcal{B}$  is the subset of buses that are neighbors to bus  $i$ . The DC-power flow is chosen to model the relationship between line flows and bus phase angles:

$$P_{ij} = B_{ij}(\theta_i - \theta_j) \quad \forall \{i,j\} \in \mathcal{E}. \quad (9)$$

From (9), the net line flow injection at any bus  $i \in \mathcal{B}$  is defined by the  $i^{\text{th}}$  element of the product of the graph Laplacian ( $L$ ) and the vector  $\theta$ :

$$P_{\text{Line}}^i = -[L\theta]_i. \quad (10)$$

For buses without a generator, the bus angles and frequencies are governed by the following:

$$\Pi_L L \theta = \Pi_L P_{\text{sh}} + \Pi_L \eta, \quad (11)$$

where  $\Pi_L$  is the non-generator bus selection matrix satisfying  $\theta_L = \Pi_L \theta$ . Differentiating (12), the frequency dynamics at non-generating buses are given by:

$$\Pi_L L \dot{\theta} = (2\pi f_{\text{base}}) \Pi_L L \omega = \Pi_L \dot{P}_{\text{sh}} + \Pi_L \dot{\eta}. \quad (12)$$

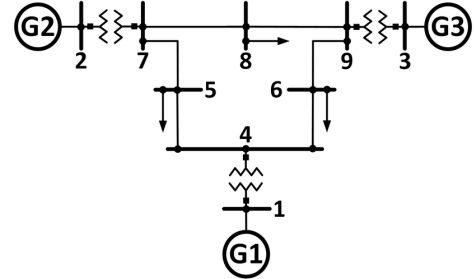


**Figure 1. WECC 9 Bus System.**

In UFLS applications,  $P_{\text{sh}}$  and  $\eta$  are step inputs to the system model equations, which implies that their derivatives are impulse functions that are non-zero for only an infinitesimal time duration. This simplifies the non-generator equations to the following expression Figliolo and Giusto, 2020:

$$(2\pi f_{\text{base}}) \Pi_L L \omega = 0. \quad (13)$$

Combining the bus frequencies can be expressed as a set of Differential Algebraic Equations (DAEs), where  $\theta_G$ ,  $\theta_L$ ,  $\omega_G$  and  $\omega_L$  are governed by (11), (13) and

$$\begin{bmatrix} \dot{\theta}_G \\ \dot{\omega}_G \\ \dot{x}_{\text{gov}} \end{bmatrix} = \begin{bmatrix} \mathbf{0} & A_{12} & \mathbf{0} \\ A_{21} & A_{22} & A_{23} \\ \mathbf{0} & A_{32} & A_{33} \end{bmatrix} \begin{bmatrix} \theta \\ \omega \\ x_{\text{gov}} \end{bmatrix} + \begin{bmatrix} \mathbf{0} \\ \Pi_G \\ \mathbf{0} \end{bmatrix} P_{\text{sh}} + \begin{bmatrix} \mathbf{0} \\ \Pi_G G \\ \mathbf{0} \end{bmatrix} \eta, \quad (14)$$

where block matrices  $A_{ij}$  are defined as

$$A_{12} := (2\pi f_{\text{base}}) \Pi_G \quad A_{21} := -M^{-1} \Pi_G$$

$$A_{22} := -M^{-1} D \Pi_G \quad A_{23} := -M^{-1} K_{\text{gov}}$$

$$A_{32} := T_{\text{gov}}^{-1} \Pi_G \quad A_{33} := -T_{\text{gov}}^{-1}.$$

The differential equation (14) is then discretized in time using trapezoidal integration, which yields the difference equation

$$\begin{aligned} x[t_{n+1}] \approx & x[t_n] + \frac{\Delta t}{2} (Ax[t_{n+1}] + BP_{\text{sh}}[t_{n+1}] \\ & + G\eta[t_{n+1}] + Ax[t_n] + BP_{\text{sh}}[t_n] + G\eta[t_n]), \end{aligned} \quad (15)$$

where vector  $x^{\top} := \text{col}\{\theta^{\top}, \omega^{\top}, x_{\text{gov}}^{\top}\}$  and matrices  $A, B$ , and  $G$  are from (15).

Next, we validate the simplified, DC-based model of the bulk power system dynamics. Then, we incorporate the simplified model into an mixed-integer programming formulation to determine optimal UFLS parameters.

### 3. Model Validation

The simplified, linearized DAE model presented in the previous section is validated against the full nonlinear dynamics model using the WECC 9 bus system (shown in Fig.1). The validation is conducted via the Power System Analysis Toolbox (PSAT) Vanfretti and Milano, 2010, which considers the nonlinear AC power flow equations, swing equations, governor dynamics, automatic voltage regulator, higher order generator model, and converted constant power load models. The WECC 9 bus system parameters were

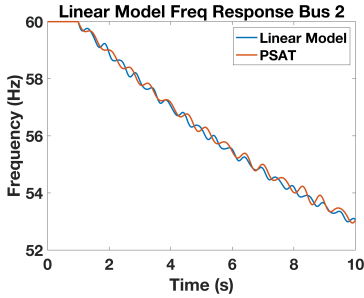


**Figure 2. Model Validation without governor action.**

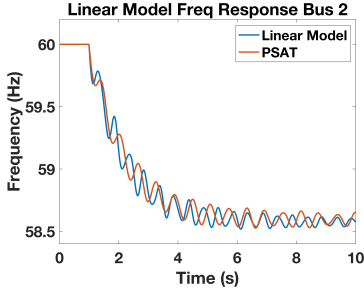


**Figure 3. Model Validation with governor action.**

obtained from PSAT. In determining how well the linear model captures the dominant nonlinear PSAT modes, the focus of validation is on the bus frequencies. Two scenarios are set up for validation and each considers a 0.50pu disturbance (e.g., lost generation) and 1) without and 2) with governor action. From Figs. 2 and 3, it is clear that Bus 2 frequency response is sufficiently accurate with the simplified model for the purpose of the UFLS scheme design in this paper.

The linear model mimics the overall frequency trend well from the nonlinear dynamics model, for both scenarios (with and without governor action). The small discrepancies in the bus frequency can be accounted for by the choice of DC power flow (used in our model) vs AC power flow network constraints in simplified vs. PSAT approach.

#### 4. Optimization Formulation

The linear model discussed in Section 2 is used for UFLS scheme design in our approach. The UFLS scheme is defined by setpoints that include the amount of load to be shed at each bus (with non-zero loads) and the frequency thresholds at which load-shedding action should actuate. We develop and use a MILP formulation to find the optimal frequency thresholds, amount of load shed and location of load shed for a given disturbance  $\eta(t)$ . We extend the analysis across a set of disturbances. The following objective function is used:

$$\min \sum_{k=1}^K \|\omega[k]\|_1 + \gamma^T P_{\text{sh}}[k]. \quad (16)$$

The first term in the objective function shown in (16) is the  $L_1$  norm of the vector  $\omega[k]$  containing all the frequency deviations from nominal for all the buses at timestep  $k$ . The second term penalizes any load shed to arrest the frequency

decline and can be used to prioritize certain loads over others in the UFLS scheme.  $\gamma$  is a vector with each element,  $\gamma_n$ , representing the cost associated with shedding load at bus  $n$ . Increasing the value of  $\gamma_n$  would increase the cost associated with shedding load at bus  $n$  and enables prioritization of load shedding at certain buses in the system.

#### 4.1. UFLS Practical System Implications

In a UFLS scheme, the load is shed in discrete amounts and only after the bus frequency falls below a specific threshold frequency. A UFLS scheme usually includes multiple stages, each with an associated amount of load-shed and a corresponding frequency threshold. Also, for the timescale of the disturbance, the shed load is not reconnected back into the system. This means that the amount of load shed should be non-decreasing over time. Furthermore, to account for noise in frequency measurement, the load is not shed based on instantaneous frequency values; instead, a deadband is added to ensure that the load shedding only occurs after being below a frequency threshold for a given time (100-200 ms). In addition, UFLS relays cannot instantaneously trigger a circuit breaker, and a delay between relay tripping and circuit breaker actuation needs to be considered (100ms). Amraee et al., 2017 and Rafinia et al., 2020 considers these practical constraints by introducing two binary variables. One of the binary variables indicates whether the frequency is below the threshold, and the second models the deadband and only becomes 1 if the frequency is below the threshold for more than the deadband time. Extending these formulations to include the network information increases the number of binary variables by a factor of  $N$ , where  $N$  is the number of buses. This paper ensures the UFLS practical constraints are met with half as many binary variables, reducing computational complexity significantly. Moreover, the underlying problem formulation is a computationally tractable MILP problem compared to the non-convex formulation in Amraee et al., 2017 and Rafinia et al., 2020. We describe the problem physics here with the following mixed-integer constraints:

$$\omega_{\text{sh}}^i - \omega_n[k] - \sum_{l=1}^{k-1} \alpha_n^i[l] \leq \alpha_n^i[k] \leq 1 + \omega_{\text{sh}}^i - \omega_n[k] \quad (17a)$$

$$\sum_{k=1}^K \alpha_n^i[k] \leq K_{db} := \frac{t_{db}}{t_s} \quad (17b)$$

$$0 \leq P_n^i[k+1] - P_n^i[k] \leq \bar{P} \alpha_n^i[k-z] \quad (17c)$$

$$p_{\text{sh}}[k+t_{\text{delay}}] = \sum_{i=1}^{N_{UFLS}} P_n^i[k] \quad (17d)$$

$$P_n^i[1] = 0 \quad (17e)$$

$$\alpha_n^i[1] = 0 \quad (17f)$$

$$\alpha_n^i[k] \in \{0,1\} \quad (17g)$$

for  $i = 1, \dots, N_{\text{UFLS}}$ ,  $k = 1, \dots, K$ ,  $n = 1, \dots, N_L$ , and  $z = 0, \dots, K_{db} - 1$ , where  $N_{\text{UFLS}}$  is the number of load shedding stages in the UFLS scheme,  $K$  is the total number of timesteps,  $N_L$  is the number of load buses available for UFLS, and  $K_{db}$  is the number of timesteps in the deadband. Decision variable  $\omega_{\text{sh}}^i$  is the frequency threshold for the  $i^{\text{th}}$  UFLS load shedding stage and  $\omega_n[k]$  the predicted frequency at bus  $n$  and  $t_{db}$  is the deadband time. The sampling time is denoted  $t_s$  and  $P_n^i[k]$  is the optimal amount of load shed at bus  $n$  in the  $i^{\text{th}}$  UFLS stage.

The constraints (17a) and (17f) ensure that  $\alpha_n^i[k]$  is zero if  $\omega_n[k] \geq \omega_{\text{sh}}^i$ . Constraint (17b) ensures that there can at most be  $K_{db}$  non-zero  $\alpha_n^i[k]$  over all timesteps, meaning that load shed can only occur once per UFLS stage. Constraints (17c) and (17e) ensure that the load shed in the  $i^{\text{th}}$  UFLS stage can only become non-zero, if  $\alpha_n^i[k]$  is non-zero for  $K_{db}$  consecutive timesteps, which means that the predicted bus frequency is below the threshold for at least  $K_{db}$  timesteps. Lastly, (17d) ensures that the load shed at a bus is equal to the sum of the load shed at each UFLS stage, with an explicit delay to capture the time between the UFLS relay triggering and circuit breaker actuation.

## 4.2. DER Implications

With the prevalence of DERs such as residential PV, both load and generation downstream of a UFLS relay exist. Thus, when UFLS trips, it is the net load (i.e., the difference between load and generation) that trips. During peak PV generation and light load times, DER generation can exceed demand resulting in what is known as ‘backfeeding.’ Shedding load at that particular bus would result in a net decrease in generation rather than a decrease in load, bringing down the frequency even further. Therefore, the presence of DERs and their relative power generation compared to the load must be considered to design a UFLS scheme for the modern bidirectional power grid. Given the relative proportion of DER generation to load behind a UFLS relay ( $\beta$ ), DER power generation can be incorporated into the optimization problem formulation (17) as follows:

$$P_{\text{sh}}[k] = P_L[k] - P_{pv}[k], \quad \forall k \quad (18a)$$

$$P_{pv,n}[k] = \beta_n P_{sh,n}[k] \quad (18b)$$

where,  $P_{\text{sh}}[k]$  is the net load shed at a bus which is the difference between the load shed and the corresponding DER generation that was also lost. The coefficient  $\beta_n$  is data and computed as

$$\beta_n := \frac{P_{DER,n}}{P_{Load,n}},$$

where  $P_{DER,n}$  is the forecasted DER power generation at bus  $n$  and  $P_{Load,n}$  is the expected load power available at bus  $n$  (i.e., both are data). Note,  $\beta_n > 1$  indicates that there is back-feeding at bus  $n$ .

The following constraints ensure the non-decreasing nature

of the load shed and limit the amount of load shed at every bus:

$$P_L[k] \leq P_L^{\max} \quad \forall k \quad (19)$$

$$P_L[k+1] - P_L[k] \geq 0 \quad \forall k. \quad (20)$$

Also, bus frequency fluctuates typically as part of regular power system operation; therefore, UFLS setpoints set close to nominal frequency might trigger load shedding under normal conditions. Furthermore, a minimum gap between two consecutive frequency thresholds is needed to avoid overlap. The following constraints ensure a maximum frequency threshold and minimum frequency threshold gap:

$$\omega_{\text{sh}}^i \leq \omega_{\text{sh}}^{\max} \quad (21a)$$

$$\omega_{\text{sh}}^i - \omega_{\text{sh}}^{i+1} \geq \Delta\omega_{\min}. \quad (21b)$$

Lastly, the bus frequencies and angles should satisfy the system model equation in (15). Thus, the overall optimization problem becomes:

$$\underset{\omega_{\text{sh}}^i, P_{\text{sh}}^n}{\text{minimize}} \quad \sum_{k=1}^K \|\omega[k]\|_1 + \gamma^\top P_{\text{sh}}[k] \quad (22)$$

$$\text{subject to} \quad (15), (17) - (21) \quad (23)$$

## 5. Methodology

The optimization problem formulation in Section 4 finds the optimal location and amounts of load-shed at each stage of UFLS. It also finds the optimal frequency thresholds for the load shed for a given disturbance. According to the NERC reliability standard PRC-006, a 25% imbalance between total system load and generation is used to benchmark UFLS settings. PRC-006 lays out how long a bus frequency can be at different frequencies, with a requirement on steady-state frequency to be between 59.3 Hz and 60.7 Hz. For the time horizon considered, these requirements are met by ensuring the frequency does not go below 58.5 Hz and that a steady state frequency of 59.3 Hz and 60.7 Hz is attained. Moreover, PRC-006 mentions that the load shed for any of the UFLS stages across the entire system should not be more than 7.5% of the total load for systems with a peak load of  $\geq 100\text{MW}$ . With that, we seek to optimize the load shed location, amount of load shed per stage and frequency thresholds within the stated guidelines. A 25% load imbalance, i.e. load is increased such that there is a 25% difference between generation and load, can be applied at several different locations throughout the system. Meaning, that for a system with  $N$  buses, there are  $N$  possible locations where the load imbalance may occur resulting in  $N$  possible disturbance scenarios. Formulating the optimization problem to include all  $N$  disturbance scenarios would increase the number of binary variables by a factor of  $N$ , increasing the complexity and computational burden significantly. Therefore, we optimize each disturbance scenario separately and obtain  $N$  optimal UFLS settings. Subsequently, we find the average, maximum and minimum across all UFLS settings for each stage to make up three candidate UFLS settings. Fig.4 shows the process of obtaining the  $N$  different optimal UFLS

settings used to find the average, minimum and maximum UFLS settings. In a practical setting, the optimization for each disturbance scenario can be done in parallel.

Although, the MILP optimal UFLS setpoints yield the best performance for a specific disturbance location, practically, the disturbance location is unknown, making the direct use of the optimal UFLS setpoints impractical. Therefore, the minimum, maximum and average of all of the MILP optimal UFLS setpoints are considered. Note, it was observed that the maximum and minimum UFLS setpoints discussed earlier yielded poor performance and have a tendency to overshot and undershot respectively. Hence, the average UFLS setpoints will be considered and benchmarked against the MILP optimal of the corresponding disturbance scenario to assess the loss in optimality associated with the averaging.

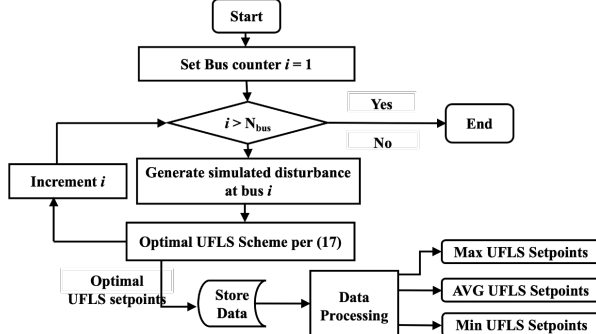


**Figure 4. Flow chart for generating optimal UFLS parameters for each scenario.**

We compare the system performance for each disturbance scenario with i) the optimal UFLS settings for that disturbance ii) the average UFLS settings, and iii) the conventional UFLS settings laid out in PRC-006. We also analyze the effect of the spatial distribution of load shed on the system performance. For this, we run a set of analyses wherein the total load shed per UFLS stage is first obtained in the case of optimal UFLS setpoints. Next, we evenly divide the load shed across various load buses resulting in a set of UFLS setpoints with an even distribution of load shed across the buses and the total load shed per UFLS stage being the same. The four sets of UFLS setpoints are summarized as follows:

1. **Optimal (MILP):** The optimal UFLS setpoints obtained from the proposed MILP optimization formulation for a given disturbance.
2. **Average:** The average of the MILP optimal UFLS setpoints obtained from all the disturbance scenarios.
3. **Conventional:** The UFLS setpoints as laid out in PRC-006 by NERC.
4. **Location Agnostic:** Obtained by even distribution/allocation of the total load shed for each UFLS stage in the MILP optimal setpoints.

## 6. Results and Discussion

We evaluate the proposed optimization-based UFLS design algorithm on the WECC 9 bus system as well as a synthetic

45 bus system. For each network case, we develop various scenarios by adding 25% of the total load (25% imbalance) to different buses in the network. For each scenario, we obtain optimal UFLS setpoints. We obtain average UFLS setpoints by averaging setpoints across all scenarios.

We use following parameters for our analyses:  $\Delta\omega_{\min} = 0.1\text{Hz}$ ,  $\omega_{\text{sh}}^{\max} = 59.5\text{Hz}$ , a dead-band of 200ms, and 100ms delay between relay trigger and circuit breaker actuation. Each load shedding stage is limited to 7.5 % of the total load and the load shed at each bus is limited to the amount of load available at the bus. The following metrics were used to assess the performance of each of the UFLS schemes in arresting the frequency decline during a disturbance:

1. **Minimum Frequency Nadir ( $f_{\text{nadir}}$ ):** Bus frequencies need to be within acceptable limits to ensure power system stability. The frequency nadir is the minimum frequency reached following a disturbance across all the buses throughout the duration of the disturbance. The frequency nadir can be calculated as follows.

$$f_{\text{nadir}} = \min_{i=1,\dots,N} \left( \min_{k=1,\dots,K} \omega_i(k) \right) \quad (24)$$

2. **Sum Absolute Error (SAE):** SAE is calculated by summing over all time-steps  $k$  the sum of the absolute frequency deviation for each bus  $i$ . The SAE penalizes frequency deviation in either direction from nominal. The mathematical expression of SAE is:

$$SAE = \sum_{i=1}^N \sum_{k=1}^K |\omega^i[k] - \omega^{nom}| \quad (25)$$

3. **Steady State Frequency ( $f_{ss}$ ):** The steady-state frequency is the frequency of the system at which it settles after a disturbance.
4. **Total Amount of Load Shed (TLS):** The total amount of load shed across all buses at the end of the time horizon considered for analyzing the disturbance (10s).

## 6.1. WECC 9 Bus System UFLS Optimization

The WECC 9 bus system has three generators and three load buses where the UFLS relay can be installed. All of the three load buses of the WECC 9 bus system are considered to be available for UFLS. Nine UFLS setpoints were obtained (one for each disturbance scenario) and the average, minimum and maximum setpoints were computed as discussed in Section 5. Table 1 shows the average frequency setpoints and load shedding amount for a system when there is no generation from DERs ( $\beta=0$ ). Fig. 5 shows the load shed amount with average, minimum and maximum UFLS setpoints. We observe that using the minimum setpoints resulted in undersheding and, conversely, the maximum setpoints led to oversheding. Therefore, the average setpoints should be considered (As shown in Table 1) Fig. 6 shows the frequency of bus 5 in with the average UFLS setpoints,

**Table 1. Realizable UFLS set-points for the 9-Bus System with the proposed Average methodology**

Frequency Threshold (Hz)	Bus 6 Load Shed (pu)	Bus 8 Load Shed (pu)	Bus 5 Load Shed (pu)
59.5	0.09	0.12	0.03
59.4	0.09	0.12	0.03
59.3	0.06	0.05	0.12
59.2	0.05	0.01	0.03

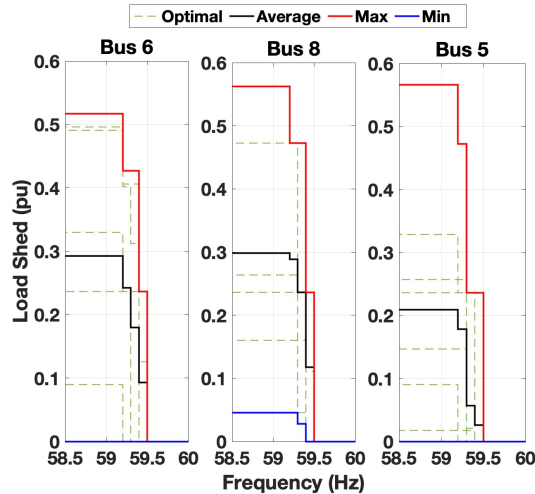


**Figure 5. UFLS settings for WECC 9 Bus without DER Generation**

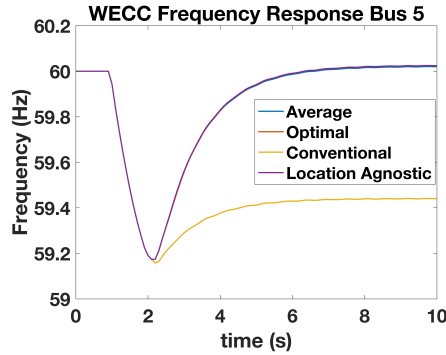


**Figure 6. Frequency Response Bus 5**

the corresponding optimal UFLS setpoints, the conventional UFLS setpoints and the location-agnostic UFLS scheme for one of the nine disturbance scenarios.

The performance metrics were calculated for each of the nine disturbance scenarios. Table 2 shows the average performance metrics across all nine scenarios without considering DER generation. The MILP optimal UFLS setpoints result in the lowest SAE as compared to the other UFLS setpoints. But applying MILP optimal UFLS scheme in the real world would mean choosing different UFLS settings for each disturbance, which is not practically realizable. Therefore, we look at average, conventional and

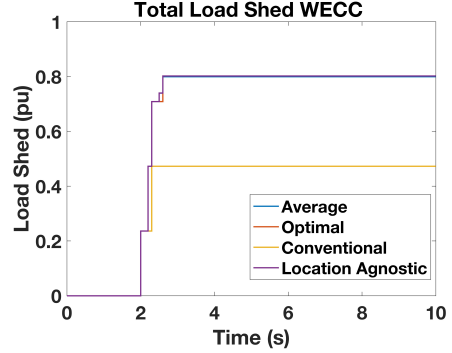


**Figure 7. Load Shedding vs Time WECC 9 Bus without DER generation**

**Table 2. WECC 9 Bus UFLS Methodology Performance Metrics**

Methodology	SAE (Hz)	$f_{\text{nadir}}$ (Hz)	$f_{\text{ss}}$ (Hz)	TLS (pu)
Conventional	500.40	59.07	59.41	0.47
Location Agnostic	170.22	59.10	59.97	0.79
Optimal (MIP)	156.92	59.10	59.99	0.80
Average	164.66	59.11	59.98	0.79

location-agnostic schemes. The average UFLS setpoints (averaging MILP optimal setpoints across all disturbances) perform better than the conventional UFLS setpoints for all performance metrics. The location-agnostic setpoints exhibit a worse SAE when compared to the average and optimal setpoints; however, the performance degradation is small. The effect of load shed location (i.e., how much load is shed where?) is more evident in the WECC 9 bus case with DER generation and the 45 bus case, as discussed later. Furthermore, both the MILP optimal, average and location-agnostic UFLS setpoints resulted in steady state frequencies almost equal to the nominal frequency, an improvement over the conventional UFLS scheme. However, we observe that the conventional scheme resulted in the least load shed and, therefore, the worst performance in terms of frequency deviation. In case of average, MILP optimal and location agnostic schemes, the amount of load shed can be controlled via choice of  $\gamma$  term in the objective function of (17)

We repeat the same experiment as before while considering DER generation at the different load buses. The  $\beta$  parameter was set to 1 for bus 5, 0.2 for bus 8 and 0 for bus 6. Table 3 contains the UFLS setpoints from average methodology with the stated values of  $\beta$ . From Table 3 it is clear that most of the load shed occurs at bus 6 with some load shed at bus 8 and none at all in bus 5. The results make intuitive sense as we should actuate UFLS at nodes with high DER generation. Bus 6 has no DER generation ( $\beta = 0$ ), making it the most suitable for UFLS. Bus 8 is less suited ( $\beta = 0.2$ ), but since  $\beta < 1$  triggering a UFLS relay at bus 8 will result in a net decrease in load. Bus 5 has  $\beta = 1$ , which indicates triggering

**Table 3. Realizable UFLS set-points for the 9-Bus System with DERs with the proposed Average methodology**

Frequency Threshold (Hz)	Bus 6 Load Shed (pu)	Bus 8 Load Shed (pu)	Bus 5 Load Shed (pu)
59.5	0.24	0	0
59.4	0.16	0.08	0
59.3	0.23	0.006	0
59.2	0.09	0.03	0

a UFLS relay at bus 5 will not affect the net load.

Fig. 8 shows the UFLS load shed amount for average, minimum and maximum settings with frequency on x-axis. We observe from the figure no load shed will occur on bus 5 due to large penetration of DERs. Fig. 9 shows the frequency of the bus 5 when the different UFLS setpoints are used and Fig. 10 shows the corresponding load shed for each of the UFLS setpoints. Table 4 summarizes the performance metrics for each UFLS setpoint with the WECC 9 bus system with DER generation. The optimal MILP UFLS setpoints again yield the best performance in terms of SAE followed closely by the average UFLS setpoints. Note, however, MILP optimal setpoints are not practically realizable and only serve as a golden benchmark. Further, note that the MILP optimal and the average UFLS setpoints result in similar SAE values. This is not the case for the conventional and location-agnostic UFLS setpoints, which show a deterioration in performance when DER generation is included. This is expected since the conventional and location-agnostic UFLS setpoints did not adapt based on the DER generation at each bus. The conventional and location-agnostic setpoints did not consider the loss in DER generation associated with shedding load at buses 5 and 8. Therefore, the amount of load that is shed is less than expected, resulting in worse performance in terms of frequency deviation (SAE).

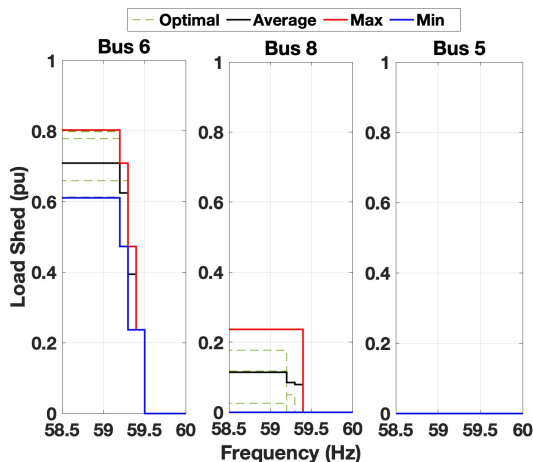


**Figure 8. Realizable UFLS set-points for the WECC 9-Bus System with DERs.**

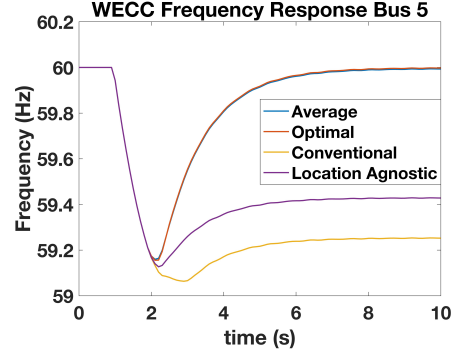


**Figure 9. Frequency Response Bus 5**

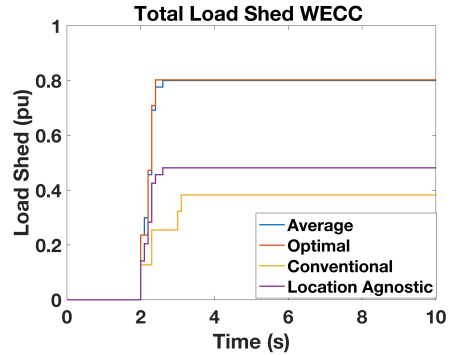


**Figure 10. Load Shedding step for WECC 9 Bus system DERs**

**Table 4. WECC 9 Bus UFLS Performance Metrics with DERs**

Methodology	SAE (Hz)	$f_{\text{nadir}}$ (Hz)	$f_{\text{ss}}$ (Hz)	TLS (pu)
Conventional	612.44	59.00	59.25	0.38
Location Agnostic	481.34	59.06	59.45	0.49
Optimal (MIP)	157.27	59.10	59.99	0.80
Average	167.07	59.10	59.97	0.79

## 6.2. Synthetic 45-Bus System

To consider the proposed methodology on a (slightly) larger system, a synthetic 45-bus system has been created by coupling together five versions of the WECC 9-bus system, which results in a system with 15 load buses (with UFLS relays) and a total load of 15.47 pu. Table 5 shows the load-shedding magnitudes and the frequency set-points for the 45-bus synthetic system with the proposed Average methodology. Fig.11 shows the frequency response of bus 5 in the system. The MILP optimal UFLS setpoints provide the minimum frequency nadir and steady-state frequency in comparison with average and conventional UFLS.

Table 6 shows the performance metrics for synthetic 45 Bus UFLS. Similar to the 9 bus case, the MILP optimal UFLS setpoints delivers the best SAE followed closely by the average UFLS setpoints. Nevertheless, the location

**Table 5. Realizable UFLS set-points for the 45-Bus System with the proposed Average methodology**

Frequency Threshold (Hz)	59.5	59.4	59.3	59.2
Bus ID	Shed (pu)	Shed (pu)	Shed (pu)	Shed (pu)
5	0.00	0.08	0.13	0.13
6	0.09	0.02	0.26	0.03
8	0.04	0.01	0.11	0.05
14	0.11	0.26	0.02	0
15	0.15	0.06	0.00	0
17	0.04	0.13	0.02	0
23	0.10	0.03	0.03	0
24	0.08	0.04	0.08	0
26	0.10	0.04	0	0
32	0.19	0.05	0	0.01
33	0.05	0.20	0	0
35	0.04	0.15	0	0
41	0.14	0.02	0.26	0.03
42	0.02	0.09	0.12	0.13
44	0.03	0.01	0.08	0.09

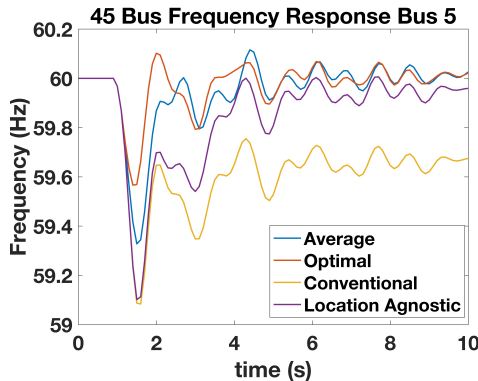


**Figure 11. Frequency Response Bus 5 in 45 bus system**

agnostic case is seen to perform significantly worse than both the MILP optimal and the average UFLS setpoints. Indicating that the location of load shed also has a significant impact on bus frequency response especially in larger networks. Furthermore, it can be observed that both the steady state frequency and frequency nadir using both the MILP optimal and average UFLS setpoints yield better frequency nadirs and steady state frequencies than the conventional and location agnostic UFLS setpoints.

### 6.3. MILP Complexity Comparison

The presented MILP formulation also improves solution efficiency by decreasing the problem's complexity. It has the advantage of having fewer binary variables and linear underlying constraints compared to other non-convex formulations with 2 binary variables (MILP with N integer

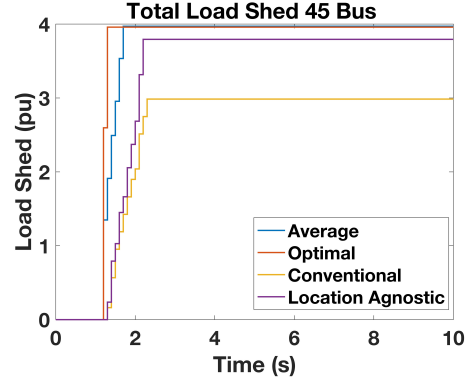


**Figure 12. Load Shedding step for 45 bus**

**Table 6. 45-Bus UFLS Methodology Performance Metrics**

Methodology	SAE (Hz)	$f_{\text{nadir}}$ (Hz)	$f_{\text{ss}}$ (Hz)	TLS (pu)
Conventional	2034.53	58.76	59.52	2.60
Location Agnostic	995.57	58.81	59.86	3.53
Optimal (MIP)	311.32	58.96	60.01	3.97
Average	318.53	58.95	60.01	3.97

**Table 7. Comparing MILP Formulations**

Network	New 1-Binary Formulation	2-Binary Formulation
	Solver Time (s)	Solver Time (s)
WECC 9 Bus	1.0	5.9
45 Bus	125.7	300.5

variables vs. MINLP with  $2N$  binary variables). To study improvement in speed, we compare the 2 binary variable formulation with our formulation. We extend the 2 binary formulation to include network information and we study the two formulations on the same disturbance scenario. This was done for both the 9 bus case and the 45 bus case. The solver times in all the cases are summarized in Table 7. We see in Table 7, a significant reduction in solving time with the 1-binary formulation presented in this paper, even for relatively small cases such as the 9 bus case.

## 7. Conclusion

A mixed-integer linear programming (MILP) formulation was presented to obtain optimal UFLS setpoints in bulk power grids that adapt with changing network conditions. The MILP formulation utilizes a linear power system model that was validated against more accurate non-linear power system dynamics simulators (PSAT). The proposed MILP formulation halves the number of binary variables necessary while still incorporating 1) conditions when the frequency

is predicted to be below a threshold and 2) triggering the load shedding action. Furthermore, the MILP formulation accounts for the network and generator physics to determine optimal UFLS parameters at each bus. The formulation also accounts for forecasted DER data (e.g., injected power) at each load bus to optimally embed UFLS participation factors into the resulting UFLS parameters. This mitigates the growing concern of triggering a UFLS relay at a load bus that is backfeeding due to DER injections, which would worsen the frequency response and could cause wide-scale blackouts.

However, despite the MILP formulation being efficient, it is still non-convex (due to binary variables), which results in a computationally complex approach. In addition, a solution is only optimal with respect to its specific, pre-determined disturbance (scenario). Thus, the MILP methodology must compute optimal solutions across all salient scenarios, but it is impractical to assume that a large disturbance can be predicted ahead of time to allow for the specific MILP solution to update all UFLS parameters in a network. To overcome this impracticality of realizing the MILP formulation, we propose a methodology that employs the average UFLS settings across all optimal solutions and illustrate on two different test networks that this approach results in near-optimal performance across all disturbance scenarios while being practically realizable.

Future work will focus on scaling up the formulation by leveraging nonlinear programming formulations such as Agarwal et al., 2022 that offer scale and can serve to provide the MILP formulation with a near-optimal, integer-feasible warm-start. Furthermore, we are interested to investigate and improve robustness of the approach by incorporating the uncertainty inherent to DER injections (i.e., account for DER forecast errors).

## References

- Adiyabazar, C., Gonzalez-Longatt, F., Acosta, M. N., Rueda, J. L., & Palensky, P. (2020). Optimal UFLS settings: An assessment of frequency system response indicators. *2020 IEEE PES Innovative Smart Grid Technologies Europe (ISGT-Europe)*, 1141–1145.
- Agarwal, A., Pandey, A., Jereminov, M., & Pillegi, L. (2022). Continuous switch model and heuristics for mixed-integer problems in power systems. *arXiv preprint arXiv:2206.14510*.
- Amraee, T., Darebaghi, M. G., Soroudi, A., & Keane, A. (2017). Probabilistic under frequency load shedding considering rocof relays of distributed generators. *IEEE Transactions on Power Systems*, 33(4), 3587–3598.
- Ceja-Gomez, F., Qadri, S. S., & Galiana, F. D. (2012). Under-frequency load shedding via integer programming. *IEEE Transactions on Power Systems*, 27(3), 1387–1394.
- Figliolo, F., & Giusto, A. (2020). Linear model for dynamic studies of power system frequency. *2020 IEEE PES Transmission & Distribution Conference and Exhibition - Latin America (T&D LA)*, 1–6.
- Ghaderi Darebaghi, M., & Amraee, T. (2017). Dynamic multi-stage under frequency load shedding considering uncertainty of generation loss. *IET Generation, Transmission & Distribution*, 11(13), 3202–3209.
- He, P., Wen, B., & Wang, H. (2019). Decentralized adaptive under frequency load shedding scheme based on load information. *IEEE Access*, 7, 52007–52014.
- Kundur, P. (1994). *Power system stability and control*. McGraw-Hill, Inc,
- Liu, Z., Wen, F., & Ledwich, G. (2014). An optimal under-frequency load shedding strategy considering distributed generators and load static characteristics. *International Transactions on Electrical Energy Systems*, 24(1), 75–90.
- Milano, F. (2017). Rotor speed-free estimation of the frequency of the center of inertia. *IEEE Transactions on Power Systems*, 33(1), 1153–1155.
- Poolla, B. K., Groß, D., Borsche, T., Bolognani, S., & Dörfler, F. (2018). Virtual inertia placement in electric power grids. *Energy Markets and Responsive Grids: Modeling, Control, and Optimization*, 281–305.
- Rafinia, A., Moshtagh, J., & Rezaei, N. (2020). Stochastic optimal robust design of a new multi-stage under-frequency load shedding system considering renewable energy sources. *International Journal of Electrical Power & Energy Systems*, 118, 105735.
- Rudez, U., & Mihalic, R. (2016). Wams-based underfrequency load shedding with short-term frequency prediction. *IEEE Transactions on Power Delivery*, 31(4), 1912–1920.
- Sigrist, L., Egido, I., & Rouco, L. (2012). Performance analysis of ufls schemes of small isolated power systems. *IEEE Transactions on Power Systems*, 27(3), 1673–1680.
- Sun, M., Liu, G., Popov, M., Terzija, V., & Azizi, S. (2021). Underfrequency load shedding using locally estimated rocof of the center of inertia. *IEEE Transactions on Power Systems*, 36(5), 4212–4222.
- Terzija, V. V. (2006). Adaptive underfrequency load shedding based on the magnitude of the disturbance estimation. *IEEE Transactions on power Systems*, 21(3), 1260–1266.
- Tofis, Y., Timotheou, S., & Kyriakides, E. (2016). Minimal load shedding using the swing equation. *IEEE Transactions on Power Systems*, 32(3), 2466–2467.
- Vanfretti, L., & Milano, F. (2010). Experience with psat (power system analysis toolbox) as free and open-source software for power system education and research. *International Journal of Electrical Engineering & Education*, 47(1), 47–62.
- Zuo, Y., Frigo, G., Derviškadić, A., & Paolone, M. (2019). Impact of synchrophasor estimation algorithms in

rocof-based under-frequency load-shedding. *IEEE Transactions on Power Systems*, 35(2), 1305–1316.